Abstract

The Southern Ocean is known as the largest High-Nutrient, Low-Chlorophyll (HNLC) region of the global ocean due to iron limitation. However, a large phytoplankton bloom develops annually downstream of the Kerguelen Islands, a bloom which is sustained partly by iron released from the sediments deposited onto the margins. In the framework of the KEOPS-2 project, we used radium isotopes (^{224}Ra, $T_{1/2} = 3.66$ d; ^{223}Ra, $T_{1/2} = 11.4$ d; ^{228}Ra, $T_{1/2} = 5.75$ y) to provide information on the origin of iron fertilization and on the timescales of the transfer of sediment-derived inputs (including iron and other micronutrients) towards offshore waters. Significant ^{224}Ra and ^{223}Ra activities were found in the near vicinity of the Kerguelen Islands, in agreement with the short half-lives of these isotopes. Significant ^{224}Ra and ^{223}Ra activities were also detected up to 200 km downstream of the islands and more unexpectedly in offshore waters south of the Polar Front. These observations thus clearly indicate i) that the sediment-derived inputs are rapidly transferred towards offshore waters (on timescales in the order of several days up to several weeks) and ii) that the Polar Front is not a physical barrier for the chemical elements released from the sediments of the Kerguelen Plateau. The Ra dataset suggests that iron and other micronutrients released by the shallow sediments of the Kerguelen margins may contribute to fuel the phytoplankton bloom downstream of the islands, despite the presence of the Polar Front. However, the heterogeneous distribution of the ^{224}Ra and ^{223}Ra activities in surface waters suggests that this supply across the front is not a continuous process, but rather a process that is highly variable in space and time.

Key words: Southern Ocean, Iron fertilization, Radium isotopes, GEOTRACES

1 Introduction

The Southern Ocean is recognized as the major High-Nutrient, Low-Chlorophyll (HNLC) region of the global ocean. Despite high nutrient concentrations, the phytoplankton growth was shown to be limited by the very low iron concentrations in surface waters of the Southern Ocean (De Baar et al., 1995; Martin et al., 1990). Dissolved iron is, however, supplied to the surface waters in several locations of the Southern Ocean where iron is released by the sediment margins but this natural iron fertilization remains spatially limited (Tagliabue et al., 2014). Consequently, high phytoplankton biomass can be found offshore the Antarctic continental shelf (Arrigo et al., 2008; Moore and Abbott, 2002) or in the vicinity of subantarctic islands (Blain et al., 2001; Korb et al., 2004; Pollard et al., 2007).

One of the largest phytoplankton blooms is observed offshore the Kerguelen Islands, in the Indian sector of the Southern Ocean (Blain et al., 2001). This phytoplankton bloom extends more than 1000 km downstream of the Kerguelen Islands and shows two main features: (i) a plume that extends northeastward of the islands and north of the Polar Front (PF) that shows high mesoscale and temporal variability, and (ii) a larger bloom southeastward of the islands and south of the PF (Blain et al., 2001, 2007). The two areas are separated by a narrow band of relatively low chlorophyll concentration associated with the PF that follows the inner shelf edge between 200 and 500 m isobaths (Park and Gamberoni, 1997; Park et al., 1998b). While Park et al. (2008a) suggest that the northward geostrophic flow associated with the PF may possibly block any southward penetration of lithogenic inputs released by the Kerguelen Islands the numerous eddies and meanders formed along the PF may contribute to transport chemical elements between the northern Kerguelen Plateau and offshore waters.

The KEOPS-2 (Kerguelen ocean and plateau compared study) project aimed at understanding the circulation patterns off the Kerguelen Islands and the mechanisms of iron fertilization in that area. The KEOPS-2 cruise was conducted during austral spring 2011 eastward of the Kerguelen Islands. Natural radio-tracers such as radium isotopes (^{223}Ra, $T_{1/2}$ = 11.4 d; ^{224}Ra, $T_{1/2}$ = 3.66 d; ^{228}Ra, $T_{1/2}$ = 5.75 y) have already been proved to be powerful tools to track the origin and fate of chemical elements - including iron and other micronutrients - that are released by the sediments deposited on the margins (Annett et al., 2013; van Beek et al., 2008; Charette et al., 2007; Dulaiova et al., 2009; Sanial et al., 2014). In this work, we refer to these latter inputs as "sediment-derived inputs". Radium isotopes are produced by the decay of particle-bound thorium isotopes in the sediments and are delivered to the open ocean by diffusion and advection processes. Thus, a water mass that interacts with shallow sediments deposited onto the margins is potentially enriched in radium and in other elements that also diffuse out of the sediments (e.g. iron, other micronutrients …). While iron may then be removed from the water column by biotic or abiotic processes, radium behaves as a conservative tracer. Radium is only affected by radioactive decay and mixing in such a way that the water body keeps the signature of its contact with the sediments. The radium signature of a given water mass may then be transferred by diffusion and advection towards offshore waters. The presence of significant Ra activities in offshore waters thus indicates that the water body has interacted with shallow sediments. Alternatively, vertical mixing may also transport Ra towards surface waters. Because radium isotopes decay, they can be used as chronometers to estimate the time elapsed since the water body left the margin, which in turn gives information on how quickly the microelements released by the shallow sediments may be transferred to offshore waters (Moore, 2000). In this work, we examined the distribution of ^{223}Ra, ^{224}Ra and ^{228}Ra in surface waters downstream of the Kerguelen Islands in order (i) to investigate the origin and dispersion of the sediment-derived inputs, including iron and (ii) to determine the apparent ages of offshore waters that provide information on the timescales of the transfer of water and associated chemical elements between the margins and offshore waters. In addition to the Ra distribution in surface waters, we report several vertical profiles of ^{223}Ra, ^{224}Ra and ^{228}Ra that provide constraints on the vertical transport of chemical elements associated with vertical mixing.

2 Material and Methods

2.1 The KEOPS-2 project

The KEOPS-2 cruise took place east of the Kerguelen Islands (northern Kerguelen Plateau) between 14 October and 23 November 2011 on board the *R/V Marion Dufresne* (IPEV: Institut Polaire Français – Paul Emile Victor and TAAF: Terres Autrales et Antarctiques Francaises). The KEOPS-2 project was designed to study the mechanisms of natural iron fertilization off Kerguelen Islands and its impact on ecosystems and biogeochemical cycles. The KEOPS-2 project was labelled as a GEOTRACES process study and followed up a first KEOPS project conducted in 2005 in the area of the Southern Kerguelen Plateau (Blain et al., 2007).

2.2 Study area

The Kerguelen Plateau, located in the Indian sector of the Southern Ocean, constitutes one of the few physical barriers for the eastward-flowing Antarctic Circumpolar Current (ACC). Various studies provide a detailed description of the general ocean circulation patterns around the Kerguelen Plateau (Charrassin et al., 2004; Park and Gambéroni, 1995; Park et al., 1998, 2008b, 2009). An important oceanographic feature of the area is the presence of the Polar Front (PF), which is commonly characterized by the northernmost position of a subsurface temperature minimum bounded by the 2 °C isotherm (Belkin and Gordon, 1996; Park and Gamberoni, 1997; Park et al., 1993). A strong eastward current associated with this front is deflected to the north at 71 °E following the eastern shelf slope of the Kerguelen Plateau between the 200 and 500 m isobaths and forms a cyclonic meander that turns southward at 75 °E (Belkin and Gordon, 1996; Orsi et al., 1995; Park and Gamberoni, 1997; Park et al., 1993; Pollard et al., 2002). Numerous eddies are generated along the PF eastward of the Kerguelen Plateau, that can, in some cases, be identified on the satellite composite images of sea surface chlorophyll. The location of the stations investigated in this study is shown on Fig. 1.

2.3 Radium data

2.3.1 Sample collection

Surface seawater samples were collected at 7 m depth using a clean pump specially designed by IPEV for the KEOPS-2 cruise. Large volumes of surface seawater were collected (250-900 L) and stored in large plastic tanks. We used a CTD (SBE-19plus, Seabird®) and a rosette system equipped with 22x12-L Niskin bottles to collect seawater samples from various depths throughout the water column. Three samples were also collected directly on two beaches of the Kerguelen Islands (Baie du Morbihan: samples KER-1 and Baie des Baleiniers: samples BaieB-1 and BaieB-2). Seawater samples were then passed by gravity through PVC cartridges filled with “Mn-fibers” (MnO_2-impregnated acrylic fiber), following (Moore, 2008). The flow rate was fixed at $\leq$ 0.5 L min^{-1} to provide 100 % extraction efficiency (Moore, 2008; van Beek et al., 2010). The Mn-fibers were then rinsed with MilliQ water and partially dried before analysis.

2.3.2 Sample analysis

The Mn-fibers were analyzed using a Radium Delayed Coincidence Counter (RaDeCC; (Charette et al., 2001; Moore and Arnold, 1996; Moore, 2008)). Three counting sessions are necessary to determine both excess ^{224}Ra and excess ^{223}Ra activities in the samples. The first counting was performed on board the research vessel during the cruise and provides the total ^{224}Ra and ^{223}Ra activities. The Mn-fibers were analyzed again 3 weeks after sampling to determine the ^{224}Ra activities supported by ^{228}Th and then after 3 months to determine the ^{223}Ra activities supported by ^{227}Ac (Moore, 2000). The ^{224}Ra activities are corrected for the ^{224}Ra supported by ^{228}Th and the ^{223}Ra activities are corrected for the ^{223}Ra supported by ^{227}Ac. The ^{224}Ra and ^{223}Ra activities discussed hereafter thus refer to these excess ^{224}Ra and ^{223}Ra activities. Uncertainties for both isotopes were calculated following Garcia-Solsona et al. (2008) and were reported with one-sigma confidence interval.

Activities of ^{228}Ra were then determined using the low-background gamma detectors placed at the LAFARA underground laboratory in the French Pyrénées (van Beek et al., 2010, 2013). Mn-fibers were either ashed at 820 °C for 16 h (Charette et al., 2001) and analyzed using a well-type germanium detector or compressed and analyzed using a semi-planar detector. Cross-calibrations between the two detectors were made to avoid any bias in the determination of the Ra activities. Each sample was analyzed for ca. 120 hours to allow the quantification of the low ^{228}Ra activities present in Southern Ocean waters (Kaufman et al., 1973). ^{228}Ra activities were determined using ^{228}Ac peaks (338, 911 and 969 keV). All radium activities are reported in disintegration per minute per 100 L of seawater (dpm/ 100 L). The uncertainties reported for gamma counting consist in the error associated with counting statistics (one sigma).

2.4 Physical data

2.4.1 Color data

High resolution maps (1/25° x 1/25°) of chlorophyll concentration (mg/ m^3) were constructed by a 10-day weighted mean of MODIS and MERIS measurements. These satellite products were delivered 3 times a week in near-real time during the cruise from Ssalto/Duacs and CLS (Collecte Localisation Satellites, Toulouse, France) with support from CNES (Centre National d'Etudes Spatiales, France). These images were used to define the sampling strategy in the investigated area.

2.4.2 Surface drifters

Drifters provided by the US National Ocean and Atmospheric Administration (NOAA) Global Drifter Program (GDP) were also released. The drogue is centered at 30 m depth. These drifters thus provide information on the mean currents in the surface mixed layer and on the dispersion of water masses due to eddy activities. Successive positions of the drifter were transmitted to the R/V Marion Dufresne four times a day by the NOAA GDP center. The time-irregular positions of the drifter were interpolated into a regular time step of 12 minutes and a low-pass filter of 48 hours was then applied to filter all tidal currents and inertial oscillations.

2.4.3 Lagrangian particle analysis

The Lagrangian particle analysis was based on total surface currents, which are the sum of the absolute geostrophic currents (deduced from altimeter product) and Ekman currents (daily mean). The Ekman component is deduced from the European Centre for Medium-Range Weather Forecasts (ECMWF) wind stress analysis applying a regional Ekman model, specifically adjusted for the Kerguelen area. The altimeter current products were produced by Ssalto/Duacs and distributed by AVISO, with support from CNES. Total surface currents were delivered every day with a 1/8° x 1/8° resolution. Details of the mapping technique are given by (Dibarboure et al., 2011).

2.4.4 Lagrangian Model

The altimetry-derived velocities providing the geostrophic mesoscale velocity at the ocean surface were analyzed in near-real time with a Lagrangian model. This model was inspired by Mongin et al. (2009) who reconstructed the extension of the Kerguelen chlorophyll plume with a transport scheme based on altimetry. The model created thousands of virtual surface drifters released on the shelf break of Kerguelen (2000 m isobaths; apparent age = 0). The trajectories were constructed by backward-in-time integration of the altimetric velocity field and were stopped when a hit over the Kerguelen shelf break was detected (indicating a trajectory coming from the shelf), or when a maximum integration time—set to 120 days—was reached (indicating no interaction with the shelf on the past 120 days). This model was applied successfully by Sanial et al. (2014) to highlight the key role played by surface horizontal transport in defining the extension of the spring-time chlorophyll plume in the Crozet area.

3 Results

3.1 Hydrological context during the KEOPS-2 cruise

The KEOPS-2 cruise lasted almost two months (October-November 2011). During that period, the phytoplankton bloom developed off the Kerguelen Islands (Fig. 2). The satellite composite images of sea surface chlorophyll reveal a complex shape of the phytoplankton bloom that may be associated with the complex hydrography of the area. High concentration of chlorophyll first appeared close to the Kerguelen Islands (October 2011) before spreading out in offshore waters until covering a large part of the study area at the end of November 2011. East of the Kerguelen Islands, a narrow band of low chlorophyll concentration is associated with the northward branch of the PF that splits the phytoplankton bloom into two parts.

The PF also delimits two surface water masses characterized by a strong contrast in temperature and salinity; the Antarctic Surface Water (AASW) is located south of the PF, and the SubAntarctic Surface Water (SASW) is located north of the PF (Emery and Meincke, 1986). The potential temperature-salinity diagrams of the water masses investigated in this study are shown in Fig. 3. The SASW is identified only at station F-L, suggesting that this station is located north of the PF. The Winter Water (WW), a typical feature of the Antarctic Zone that is characterized by a subsurface temperature minimum layer around 200 m depth (Park et al., 1998a, 2008b, 2014) is found on all the vertical profiles reported here, except for station F-L, thus confirming its location north of the PF. Below the WW, three water masses can be identified: the Upper Circumpolar Deep Water (UCDW), the Lower Circumpolar Deep Water (LCDW) and the Antarctic Bottom Water (AABW) (Park et al., 1993, 2008b). Note that the AABW is only found on the F-L profile (commonly observed below 2600 m in this area; (Park et al., 2008b)).

3.2 Radium distribution in surface waters

The radium activities reported in this study are shown in Table 1 and fall in the range of previous radium data reported for surface waters near islands of the Southern Ocean (Annett et al., 2013; Charette et al., 2007; Dulaiova et al., 2009; Hanfland, 2002; Kaufman et al., 1973; Sanial et al., 2014; van Beek et al., 2008). The highest ^{223}Ra, ^{224}Ra and ^{228}Ra activities are found in seawater samples collected at shallow stations near the Kerguelen Islands (bathymetry < 200 m; Fig. 4). The radium activities then gradually decrease offshore. Several samples, however, display significant ^{224}Ra activities in samples collected offshore (Fig. 4a): stations UW-21-23-34 and TEW-7 located along the PF; stations UW-32, E-1 and TEW-5 south of the PF; and station TNS-1 north of the PF. A greater number of offshore stations exhibit significant ^{223}Ra activities, which agrees with the longer half-life of the ^{223}Ra isotope (Fig. 4b). The stations displaying significant ^{224}Ra activities also display significant

^{223}Ra activities. The radium activities are especially high at station TNS-2 located north of the PF and at stations E-1 and G-1, located south of the PF. Station G-2 was visited twice and showed high ^{223}Ra and ^{224}Ra activities at both visits. Station A3 located on the southern Kerguelen Plateau was also visited twice. Significant ^{223}Ra and ^{224}Ra activities were determined in the water sample collected at station A3-1 during the first visit at station A3 (note however that these activities are low) but were both below the detection limit at station A3-2 (second visit at station A3). In contrast, the ^{228}Ra activities are similar at the two visits of A3 (Table 1). All surface samples display significant ^{228}Ra activities up to ca. 300 kilometers offshore from the Kerguelen Islands (i.e. station TEW-8). Relatively high values are observed at stations TNS-2 and UW-32 located north and south of the PF, respectively (Fig. 4c). Station R-2, which was chosen as the reference station for typical HNLC waters east of the Kerguelen Islands, shows significant ^{223}Ra, ^{224}Ra and ^{228}Ra activities in surface waters.

3.3 Vertical distribution of Ra isotopes

The study of the vertical distribution of Ra isotopes allows us to provide constraints on the vertical transport of Ra associated with vertical mixing. Consequently, these profiles help us to define the origin of the Ra enrichments observed in surface waters off the Kerguelen Islands (lateral versus vertical supply of Ra). The major water masses, identified with the potential temperature-salinity diagrams throughout the water column are reported for each profile. The shallow Ra profiles (stations TEW-3, G-1 and A3-2) are shown on Fig. 5 and the deep profiles (stations F-L, E-4W and E-1) are shown on Fig. 6.

The ^{223}Ra and ^{224}Ra activities are usually higher in samples collected near the seafloor and are below the detection limit at intermediate depths (Table 2; Fig. 5 and 6). Significant ^{223}Ra and ^{224}Ra activities are observed in surface and/or subsurface waters several kilometers offshore from the islands, in particular at stations G-1 and E-1 located south of the PF and at station F-L located north of the PF. The vertical profiles of ^{223}Ra and ^{224}Ra are quite unique at station F-L. Although i) this station is located far from the Kerguelen Islands and ii) the bottom is at 2670 m depth, the ^{223}Ra and ^{224}Ra activities are relatively high throughout the water column (Fig. 6). Significant ^{228}Ra activities were found in the different water columns investigated in this study. The ^{228}Ra activities at stations TEW-3 and G-1 are relatively high and uniform throughout the water column. The ^{228}Ra activities at station A3 are uniform in the upper 250 m and then increase with increasing water depth. The vertical ^{228}Ra profiles at the deep stations (F-L, E-1 and E-4W) exhibit an increasing trend with increasing depth reflecting the diffusion of radium out of the sediments. This latter pattern is also especially marked at station A3 on the southern Kerguelen Plateau (Fig. 5).

4. Discussion

4.1 Origin of the radium enrichments in surface waters

The relatively high radium activities (^{223}Ra, ^{224}Ra and ^{228}Ra) observed in surface waters east of the Kerguelen Islands may be explained either by the vertical transport or diffusion that supplies radium to surface waters or by the lateral advection of waters that have recently interacted with shallow sediments (Blain et al., 2001; Park et al., 2008a, van Beek et al., 2008).

When considering solely the ^{228}Ra vertical profiles - that show in most cases an increase of ^{228}Ra activities with increasing depth - it cannot be excluded that the vertical mixing contributes to increase radium activities in surface waters. However, the ^{224}Ra and ^{223}Ra vertical profiles – that show higher Ra activities in the upper and in the deep water column but Ra activities below the detection limit in the mid water column - clearly indicate that the higher ^{224}Ra and ^{223}Ra activities in surface waters cannot be explained by vertical mixing. The

^{224}Ra and ^{223}Ra enrichments in surface waters are thus more likely explained by the lateral advection of waters that have recently interacted with shallow sediments.

The northward advection of a water mass that has interacted with the shallow sediments deposited on the shelves of Heard Island has been identified as a pathway for the micronutrients that sustain the phytoplankton bloom on the southern Kerguelen Plateau (Chever et al., 2010; van Beek et al., 2008; Zhang et al., 2008). The presence of a chlorophyll plume that expands northward of the southern Kerguelen Plateau may also support the existence of this northward advection (Fig. 2). The observation of significant ^{224}Ra and ^{223}Ra activities in surface waters at station A3-1 confirms this circulation pattern and suggests that the transit time of the waters that interacted with the shallow margins of Heard Island may be <1 month between Heard Islands and station A-3. This is in agreement with the Ra data obtained in 2005 during the KEOPS-1 project, where significant ^{224}Ra and ^{223}Ra activities were also found in surface waters at station A3 (van Beek et al., unpublished data). When the waters move further north towards the area investigated in this study, the ^{224}Ra and ^{223}Ra activities will then continue to decay. Two drifters released during the KEOPS-2 cruise at station A3 allow us to provide constraints on the transit time between the southern Kerguelen Plateau and the studied area (eastward of Kerguelen at around 49 °S). A first drifter recirculated around station A3 nearly 20 days before it moved slowly northward. It took approximately 60-75 days for the drifter to reach the investigated area located eastward of the Kerguelen Islands (Fig. 7). It took approximately 53-65 days for the second drifter to reach the area eastward of Kerguelen. Such transit times agree with the estimate of Park et al. (2008b) during the KEOPS-1 project (i.e. several months between Heard Islands and the eastern flank of the Kerguelen Islands). With such a transit time, a water body that interacted with the shallow margins of Heard Island should not contain any remaining short-lived radium isotopes when reaching the eastern flank of the Kerguelen Islands. As a consequence, the ^{224}Ra and ^{223}Ra activities found in offshore waters east of the Kerguelen Islands, south of the PF are best explained by diffusion or advection of Ra via waters that recently interacted with the shallow sediments of the northern Kerguelen Plateau. This scenario, however, implies that the Ra isotopes (and potentially other chemical elements such as iron) were transferred offshore across or via the PF. High dissolved and particulate trace element concentrations (Fe, Ni and Co) were also found east of the PF confirming that chemical elements may be transported offshore across or via the PF (Quéroué et al. 2014; van der Merwe et al., 2014). Among the potential mechanisms allowing surface waters to be transported eastward across the PF, one can invoke either i) the wind stress (eastward winds are especially strong in that region) or ii) eddies that form along the PF and that could promote the passage of chemical elements across the front.

However, a contribution of surface waters originating from the southern Kerguelen Plateau may not be completely excluded. In contrast to ^{224}Ra and ^{223}Ra that both disappear due to radioactive decay along the northward transport, ^{228}Ra with a longer half-life would remain in these waters. The ^{228}Ra activities observed eastward of the Kerguelen Islands may thus be partly explained by an advective transport of waters originating from the south. It cannot be excluded, therefore, that the northward advection originating from the southern plateau contributes to the natural fertilization of the investigated area, in addition to the input of chemical elements across the PF that was shown by the short lived isotopes.

South of the Kerguelen Islands (i.e. along the Polar Front at stations UW-23 and UW-24 or south of the Polar Front e.g. at stations UW-15, UW-16, R-2; Figure 4), it cannot be completely excluded that the observed radium enrichments are partly explained by an input of radium associated with the Leclaire Rise located west of the Kerguelen Islands at ca 350 m depth (Weis and Frey, 2002). Station R-2, which is located east of the Leclaire Rise south of the Polar Front, shows significant ^{223}Ra and ^{224}Ra activities in surface waters. Although these activities are relatively low (0.016 and 0.057 dpm/ 100 L, respectively), they suggest that the waters downstream of the Leclaire Rise may be impacted by this topographic feature. However, sample UW-14 collected in surface waters lying above this rise does not show significant ^{223}Ra and ^{224}Ra activities and only low ^{228}Ra activity, which suggest that vertical mixing may not efficiently transport radium released by the shallow sediments towards surface waters above this topographic feature. Note that the influence of the Leclaire Rise on the chemical element concentrations downstream of the rise is also observed in Fe and other trace metal (REE, Mn, Al) concentrations, but only in waters lying in the 200-500 m depth interval (Bowie et al., 2014; van der Merwe et al., 2014; Grenier et al., in prep.).

4.2 Timescales of the offshore transport of surface waters

Once released into the water column, radium isotopes are subject to dilution, mixing and radioactive decay. The decay of short-lived radium isotopes in offshore waters provides information of how quickly chemical elements (including micronutrients) also released by the sediments are diluted and dispersed into the ocean (Moore, 2000). The presence of ^{224}Ra and ^{223}Ra in offshore waters thus indicates that the waters have recently been in interaction with the sediments. In contrast, when both ^{224}Ra and ^{223}Ra activities are below the detection limit, this suggests that the water bodies have not been in contact with the sediments over the past 2 months (this is represented in light gray in Fig. 8). The water samples that display significant ^{223}Ra activity but no ^{224}Ra (represented in dark gray in Fig. 8) suggest that the interaction between the water body and the sediment occurred between 1 month (^{224}Ra activities < DL) and 2 months ago (significant ^{223}Ra activities). When both the ^{224}Ra and ^{223}Ra activities were significant, apparent ages could be calculated following (Moore, 2000) :

$$t = \ln \frac{\left[\frac{^{224}\mathrm{Ra}}{^{223}\mathrm{Ra}}\right]_i}{\left[\frac{^{224}\mathrm{Ra}}{^{223}\mathrm{Ra}}\right]_{obs}} * \frac{1}{\lambda_{224}-\lambda_{223}} \qquad (1)$$

where $(^{224}Ra/^{223}Ra)_i$ is the initial ratio in source waters, $(^{224}Ra/^{223}Ra)_{obs}$ is the ratio for a given water sample, λ_{224} and λ_{223} are the decay constants of ^{224}Ra and ^{223}Ra, respectively. The assumptions inherent to this equation can be found in Moore (2000) and are: (1) the ^{223}Ra and ^{224}Ra activities are constant in the source region (i.e. a constant initial $^{224}Ra/^{223}Ra$ ratio is assumed), (2) the $^{224}Ra/^{223}Ra$ ratio changes are only due to radioactive decay and (3) open ocean waters contain no excess ^{223}Ra and ^{224}Ra.

In this study, we only reported the apparent ages deduced from the $^{224}Ra/^{223}Ra$ ratios because we showed that both the ^{224}Ra and ^{223}Ra determined eastward of Kerguelen originate from the shallow sediments of the Kerguelen Islands (see section 4.1). Apparent ages were thus calculated using an initial $^{224}Ra/^{223}Ra$ ratio that was obtained by averaging the ratios found in coastal water samples collected as close as possible to the radium source term in the Baie du Morbihan (samples KER-1 and UW-36) and Baie des Baleiniers (samples Baie-B1 and Baie-B2; Fig. 1). In contrast, we cannot exclude that ^{228}Ra has various origins (Kerguelen Islands and/or Heard Island). The use of the $^{224}Ra/^{228}Ra$ or $^{223}Ra/^{228}Ra$ ratios to derive apparent ages is thus compromised because it is not possible to determine a single initial ratio in this case.

Several offshore samples display a young apparent age (4-8 days), suggesting a rapid transport of radium between the shallow waters of the northern Kerguelen Plateau and offshore. Station TNS1 located north of the PF is reached after 5 days. This observation agrees with the circulation pattern in this area, with waters flowing eastward and that may interact with the shallow northern Kerguelen Plateau (Park et al., 2014). This is also in agreement with the drifters launched during the KEOPS 2 project that also highlighted such advection along the PF (Fig. 7) (Zhou et al., 2014). Station UW-21 located ca. 50 km offshore, station E1 and station UW-32 located ca. 200 km offshore also show relatively young apparent ages (4, 5 and 6 days, respectively). Because all these stations are located south of the PF, this suggests that the sediment-derived inputs may be rapidly transferred towards offshore waters across the PF. Stations R-2 located south of the PF also displays a young apparent age. At station Kerfix located close to station R-2, Jeandel et al. (1998) reported westward currents associated with a recirculation pattern that may transport chemical elements originating from the Kerguelen Plateau. The Ra signal may then be transported eastward, as suggested by the significant ^{223}Ra activities also observed east of station R-2, south of the PF (Fig. 4 and 8). Alternatively, the Leclaire Rise located west of R-2 may impact the surface waters, thus leading to a young age for this water sample. Because the ^{224}Ra and ^{223}Ra activities found at station A3-1 were attributed to the northward advection on the southern Plateau, the apparent age at station A3-1 was calculated assuming that the initial ^{224}Ra/^{223}Ra ratio off Heard Island is similar to that off Kerguelen Islands (Fig. 8). This hypothesis may be correct since the geological contexts of the two islands are similar. The apparent age thus calculated provides an estimate for the transit time of surface waters above the southern Kerguelen Plateau between Heard Island and station A3. However, during the second visit at station A3 (A3-2), the ^{224}Ra and ^{223}Ra activities were below the detection limit. This may highlight the temporal variability in the circulation patterns in this area: the transit time of surface waters between Heard Island and station A3 may thus vary with time, ranging from one week to 1-2 months. On such timescales, the ^{228}Ra activities do not significantly decay, which would explain why similar ^{228}Ra activities were found during the two visits at A3. Finally, the spatial variability in the distribution of the apparent ages in offshore waters suggests that the passage of chemical elements across the Polar Front is a sporadic process, which may contribute to explain the mosaic structure of the phytoplankton bloom. Future studies in the area could aim to track more precisely the sedimentary sources of radium (and other chemical elements) and to quantify the radium fluxes out of the sediments using e.g. the method developed by Cai et al. (2012).

4.3 Lagrangian particle analysis

To provide additional constraints on the origin of the Ra signal in offshore waters, Lagrangian analyses derived from total surface currents were conducted at several stations (Fig. 9). A two month backward analysis - to account for the life time of ^{223}Ra - was performed starting from the sampling date for targets that were centered on the station locations.

The Lagrangian analyses for the southern stations A3-1, A3-2, UW-35 and G-1 are reported on Fig. 9. The backward trajectories provide a similar pattern and indicate a southern origin for the surface waters found at these stations. This pattern agrees with the trajectories of the two drifters released *in situ* at station A3 (Fig. 7). Waters that have interacted with the shallow shelves of the southern Kerguelen Plateau (Heard Island) may thus reach the investigated area. In particular, this northward advection may explain the significant Ra activities determined at stations G-1 and A3-1. Note that the distance covered by the backward trajectories over the 2 months is short, thus reflecting the relatively slow currents in this area.

Lagrangian analyses were also performed for several northern stations: E-1, UW-31, UW-32, TEW-7 and F-L. The trajectories are represented in shades of red on Fig. 9. Stations F-L, TEW-7 and UW-31 are located relatively close to each other, east of the Kerguelen Islands in the area of the southern branch of the cyclonic meander formed by the PF. Their backward trajectories display a similar feature and all point to the same origin, which is the northern Kerguelen Plateau. This suggests that chemical elements originating from the Kerguelen Plateau may be transported offshore via the PF. The transit time given by the Lagrangian analysis is approximately one month between the coast of the Kerguelen Islands and the investigated stations. With a transit time of approximately one month, the ^{224}Ra

activities should have disappeared due to radioactive decay - or should be close to the detection limit - while the ^{223}Ra activities should have significantly decayed. As a comparison, the ^{224}Ra and ^{223}Ra activities are below the detection limit at stations F-L and UW-31, whereas significant ^{223}Ra and ^{224}Ra activities were found at station TEW-7. Such discrepancy between the investigated stations may highlight the spatial variability of the circulation patterns in this area or that the Ra activities are close to the detection limits. Both ^{224}Ra and ^{223}Ra activities are also significant at station E-1 located in the center of the cyclonic meander formed by the PF. The Lagrangian analysis suggests that the surface waters at station E-1 originate from the southwest. These waters flow northwards before reaching the PF area and then follow the eastern shelf of the northern Kerguelen Plateau. When passing close to the PF, these waters may receive significant Ra inputs (and potentially other sediment-derived inputs) that could be transported via or across the front in this area. This Ra signal may then be transferred to station E-1, as suggested by the backward trajectories. This hypothesis is also supported by the study conducted by Zhou et al. (2014) who identified a north-eastward drift of surface waters originating from the Kerguelen Plateau. Finally, the backward trajectories at station UW-32 - that also displayed significant ^{223}Ra and ^{224}Ra - highlight the spatial variability in that area: while several trajectories originate from the south, several other trajectories follow the PF and the shelves of the northern Kerguelen Plateau, where these waters could also potentially receive sediment-derived inputs.

4.4 Comparison of the apparent radium ages with an altimetry-based Lagrangian model

The timescale of the offshore transport of surface waters was also investigated using an altimetry-based Lagrangian model (Fig. 10). The color bar indicates the time (number of days) elapsed since the water body left the 2000 m-isobath. A color code similar to that of Fig. 8 was used. A color palette from red to yellow highlights the rapid offshore transport of the surface waters (surface waters < 6 days). The dark gray coding illustrates surface waters that left the 2000 m-isobath less than 1 month ago. Finally, surface waters that left the 2000 m-isobath more than 1 month ago are represented in light gray. As a comparison, the radium apparent ages are reported on the map using the same color code.

Young ages can be found close to the 2000 m-isobath, along the PF. Surface waters < 1 month follow the cyclonic meander formed by the PF, while waters older than 2 months are found in the center of the meander.Note that the altimetry-derived Lagrangian analysis may misplace structures with errors of ~10 km (e.g. d' Ovidio et al., 2010), which is comparable to the width of the structures visible in the map. It may thus be difficult to compare quantitatively the altimetry-derived ages with the ages determined *in situ*. Nevertheless, two important considerations can be made: (i) the order of magnitude of the satellite-derived and *in situ* ages are consistent in the region; (ii) considering a west-east transect from Kerguelen, both estimations indicate a transition from young to old and then again young ages, which is consistent with the existence of a retentive recirculation region centered at about 73 °W, 49 °S.

5 Conclusion

The observation of short-lived Ra isotopes (^{223}Ra and ^{224}Ra) in surface waters east of the Kerguelen Islands, south of the PF clearly indicates that these waters have recently interacted with shallow sediments. Neither the shallow margins of Heard Islands - located hundreds kilometers south of the study area - nor the vertical mixing of deep waters that interacted with bottom sediments can account for the short-lived radium enrichments found in surface waters. The ^{223}Ra and ^{224}Ra activities south of the PF are thus best explained by waters that interacted with the shallow margins of the Kerguelen Islands. This finding implies that chemical elements can be transported across or via the PF. Among the potential mechanisms allowing surface waters to be transported eastward across the PF, one can invoke either i) the wind stress (eastward winds are especially strong in that region) or ii) eddies that form along the PF and that may promote the transport of surface waters and associated chemical elements. The spatial variability observed in the ^{223}Ra and ^{224}Ra distribution in surface waters south of the PF suggests that the input of waters and associated chemical elements across the PF – potentially driven by wind stress or eddies - act as sporadic pulses that may highly vary in both space and time. This pathway may thus constitute a mechanism that contribute to fertilize the phytoplankton bloom with iron and other micronutrients east of the Kerguelen Islands, south of the PF. This finding shows that the PF may not act as a strong barrier for surface waters and associated chemical elements, a finding that may also apply to other frontal systems of the world's ocean.

Author contribution

P. van Beek and B. Lansard performed the sample collection on board the R/V Marion Dufresne. The sample analysis was done on the ship by P. van Beek and B. Lansard and in the laboratory by V. Sanial, and M. Souhaut. F. d'Ovidio developed the model code and E. Kestenare performed the CTD analysis and the simulations for the Lagrangian analysis. M. Zhou provided the drifter data. S. Blain is PI of the KEOPS-2 project and helped interpret the data. V. Sanial interpreted the data and prepared the manuscript.

Acknowledgements

The authors would like to thank Bernard Quéguiner, chief scientist of the KEOPS-2 cruise. We thank the captain and crew members of the R/V Marion Dufresne (IPEV-TAAF). We are especially grateful to Pierre Sangiardi (IPEV) who designed the clean pump that allowed us to collect surface water samples in this project. The altimeter current and color/temperature products for the Kerguelen area were produced by Ssalto/Duacs and CLS with support from CNES. This work was funded by the French Research program of INSU-CNRS LEFE-

CYBER (Les enveloppes fluides et l’environnement – Cycles biogéochimiques, environnement et ressources), ANR (Agence Nationale de la Recherche, SIMI-6 program, ANR-10-BLAN-0614), CNES (Centre National d’Etudes Spatiales) and IPEV (Institut Polaire Paul-Emile Victor).

Figure captions

Fig. 1. Location of stations investigated for Ra analysis. Solid circles represent surface seawater samples. Circles show the locations where vertical profiles were made. KP is the abbreviation for Kerguelen Plateau.

Fig. 2. Satellite composite images of sea surface chlorophyll *a* (mg m^{-3}) at successive dates between the beginning of the KEOPS-2 cruise (19/10/2011) and the end of the cruise (23/11/2011). The location of the water samples collected for radium analysis within the different time intervals is also reported (solid circles).

Fig. 3. Potential temperature-salinity diagrams at stations where radium analyses were performed. F-L station is plotted in bold. TEW-3, G-1, E-1, E4-W and A3-2 stations are plotted in gray. The main water masses are reported on the figure: Antarctic Surface Water (AASW), SubAntarctic Surface Water (SASW), Winter Water (WW), Upper Circumpolar Deep Water (UCDW), Lower Circumpolar Deep Water (LCDW) and Antarctic Bottom Water (AABW).

Fig. 4. ^{224}Ra (A), ^{223}Ra (B) and ^{228}Ra (C) distributions in surface waters off the Kerguelen Islands. Radium activities are expressed in dpm/ 100 L. White circles indicate samples with Ra activity below the detection limit. A schematic view of the Polar Front (PF) is shown.

Fig. 5. Vertical profiles of ^{223}Ra, ^{224}Ra and ^{228}Ra activities (dpm/ 100 L) at the shallow stations. The main water masses are indicated: Winter Water (WW), Upper Circumpolar Deep Water (UCDW). The bottom depth is denoted by the horizontal lines.

Fig. 6. ^{223}Ra, ^{224}Ra and ^{228}Ra activities (dpm/ 100 L) at the deep stations. The major water masses are indicated: Winter Water (WW), Upper Circumpolar Deep Water (UCDW), Lower

Circumpolar Deep Water (LCDW), Antarctic Bottom Water (AABW). The bottom depth is denoted by the horizontal lines.

Fig. 7. Trajectories of the drifters launched eastward of the Kerguelen Islands during the KEOPS-2 project. The trajectories of the two drifters released at station A3 are reported in color. The equivalent transit time of the two drifters is reported in days along their trajectory. The other drifter trajectories are represented in light grey.

Fig. 8. Apparent ages of surface waters determined using the ^{224}Ra/^{223}Ra ratios. The offshore apparent ages were estimated using an initial ^{224}Ra/^{223}Ra ratio that was obtained by averaging the ratios found at stations located on the northern Kerguelen Plateau (< 200 m water depth). When both ^{224}Ra and ^{223}Ra were significant, apparent ages could be determined (colored symbols). The samples displaying an apparent age between 1 and 2 months are shown in dark gray (^{224}Ra < DL but significant ^{223}Ra activities). Water samples displaying an apparent age > 2 months are shown in light grey (^{224}Ra < DL and ^{223}Ra < DL). A schematic view of the Polar Front (PF) is represented.

Fig. 9. Lagrangian particle analysis derived from total surface currents (considering absolute geostrophic plus Ekman currents). Solid circles represent the location of the stations. The targets for Lagrangian analysis were centered on and around the station locations (to account for spatial variability). The sampling date is indicated in brackets. Two month-backward trajectories are shown. The first month is represented in bold.

Fig. 10. Ages of surface waters (in days) derived from an altimetry Lagrangian-based model. *In-situ* ages derived from radium isotopes are represented by circles. The colorbar indicates the time elapsed since the water body left the 2000-m isobath.

References

Annett, A. L., Henley, S. F., Van Beek, P., Souhaut, M., Ganeshram, R., Venables, H. J., Meredith, M. P. and Geibert, W.: Use of radium isotopes to estimate mixing rates and trace sediment inputs to surface waters in northern Marguerite Bay, Antarctic Peninsula, Antarctic Science, FirstView, 1–12, doi:10.1017/S0954102012000892, 2013.

Arrigo, K. R., Van Dijken, G. L. and Bushinsky, S.: Primary production in the Southern Ocean, 1997–2006, Journal of Geophysical Research: Oceans, 113(C8), doi:10.1029/2007JC004551, 2008.

De Baar, H. J. W., De Jong, J. T. M., Bakker, D. C. E., Löscher, B. M., Veth, C., Bathmann, U. and Smetacek, V.: Importance of iron for plankton blooms and carbon dioxide drawdown in the Southern Ocean, Nature, 373(6513), 412–415, doi:10.1038/373412a0, 1995.

Belkin, I. M. and Gordon, A. L.: Southern Ocean fronts from the Greenwich meridian to Tasmania, Journal of Geophysical Research: Oceans, 101(C2), 3675–3696, doi:10.1029/95JC02750, 1996.

Blain, S., Quéguiner, B., Armand, L., Belviso, S., Bombled, B., Bopp, L., Bowie, A., Brunet, C., Brussaard, C., Carlotti, F., Christaki, U., Corbière, A., Durand, I., Ebersbach, F., Fuda, J.-L., Garcia, N., Gerringa, L., Griffiths, B., Guigue, C., Guillerm, C., Jacquet, S., Jeandel, C., Laan, P., Lefèvre, D., Lo Monaco, C., Malits, A., Mosseri, J., Obernosterer, I., Park, Y.-H., Picheral, M., Pondaven, P., Remenyi, T., Sandroni, V., Sarthou, G., Savoye, N., Scouarnec, L., Souhaut, M., Thuiller, D., Timmermans, K., Trull, T., Uitz, J., Van Beek, P., Veldhuis, M., Vincent, D., Viollier, E., Vong, L. and Wagener, T.: Effect of natural iron fertilization on carbon sequestration in the Southern Ocean, Nature, 446(7139), 1070–1074, doi:10.1038/nature05700, 2007.

Blain, S., Tréguer, P., Belviso, S., Bucciarelli, E., Denis, M., Desabre, S., Fiala, M., Martin Jézéquel, V., Le Fèvre, J., Mayzaud, P., Marty, J.-C. and Razouls, S.: A biogeochemical study of the island mass effect in the context of the iron hypothesis: Kerguelen Islands, Southern Ocean, Deep Sea Research Part I: Oceanographic Research Papers, 48(1), 163–187, doi:10.1016/S0967-0637(00)00047-9, 2001.

Bowie, A. R., Van der Merwe, P., Quéroué, F., Trull, T., Fourquez, M., Planchon, F., Sarthou, G., Chever, F., Townsend, A. T., Obernosterer, I., Sallée, J.-B. and Blain, S.: Iron budgets for three distinct biogeochemical sites around the Kerguelen archipelago (Southern Ocean) during the natural fertilisation experiment KEOPS-2, Biogeosciences Discuss., 11(12), 17861–17923, doi:10.5194/bgd-11-17861-2014, 2014.

Cai, P., Shi, X., Moore, W. S. and Dai, M.: Measurement of 224Ra:228Th disequilibrium in coastal sediments using a delayed coincidence counter, Marine Chemistry, 138–139, 1–6, doi:10.1016/j.marchem.2012.05.004, 2012.

Charette, M. A., Buesseler, K. O. and Andrews, J. E.: Utility of radium isotopes for evaluating the input and transport of ground-water-drived nitrogen to a Cape Cod estuary, Limnology and oceanography, 46(2), 465–470, 2001.

Charette, M. A., Gonneea, M. E., Morris, P. J., Statham, P., Fones, G., Planquette, H., Salter, I. and Garabato, A. N.: Radium isotopes as tracers of iron sources fueling a Southern Ocean phytoplankton bloom, Deep Sea Research Part II: Topical Studies in Oceanography, 54(18–20), 1989–1998, doi:10.1016/j.dsr2.2007.06.003, 2007.

Charrassin, J.-B., Park, Y.-H., Le Maho, Y. and Bost, C.-A.: Fine resolution 3D temperature fields off Kerguelen from instrumented penguins, Deep Sea Research Part I: Oceanographic Research Papers, 51(12), 2091–2103, doi:10.1016/j.dsr.2004.07.019, 2004.

Chever, F., Sarthou, G., Bucciarelli, E., Blain, S. and Bowie, A. R.: An iron budget during the natural iron fertilisation experiment KEOPS (Kerguelen Islands, Southern Ocean), Biogeosciences, 7(2), 455–468, doi:10.5194/bg-7-455-2010, 2010.

Dibarboure, G., Pujol, M.-I., Briol, F., Traon, P. Y. L., Larnicol, G., Picot, N., Mertz, F. and Ablain, M.: Jason-2 in DUACS: Updated System Description, First Tandem Results and Impact on Processing and Products, Marine Geodesy, 34(3-4), 214–241, doi:10.1080/01490419.2011.584826, 2011.

Dulaiova, H., Ardelan, M. V., Henderson, P. B. and Charette, M. A.: Shelf-derived iron inputs drive biological productivity in the southern Drake Passage, Global Biogeochemical Cycles, 23(4), n/a–n/a, doi:10.1029/2008GB003406, 2009.

Emery, W. J. and Meincke, J.: Global water masses: summary and review, Oceanologica acta, 9(4), 383–391, 1986.

Garcia-Solsona, E., Garcia-Orellana, J., Masqué, P. and Dulaiova, H.: Uncertainties associated with 223Ra and 224Ra measurements in water via a Delayed Coincidence Counter (RaDeCC), Marine Chemistry, 109(3–4), 198–219, doi:10.1016/j.marchem.2007.11.006, 2008.

Grenier, M., Garcia-Solsona, E., Lemaitre, N., Bouvier, V., Nonnotte, P., Jeandel, C. : Differentiating lithogenic supplies, water mass transport and biological processes on and off the Kerguelen Plateau using the rare earth data, in prep.

Hanfland, C.: Radium-226 and Radium-228 in the Atlantic Sector of the Southern Ocean, thesis, Alfred Wegener Institute, Bremerhaven Allemagne., 2002.

Jeandel, C., Ruiz-Pino, D., Gjata, E., Poisson, A., Brunet, C., Charriaud, E., dehairs, F., delille, D., Fiala, M., Fravalo, C., Carlos Miquel, J., Park, Y., Pondaven, P., Queguiner, B., Razouls, S., Shauer, B. and Treguer, P.: KERFIX, a time-series station in the Southern Ocean: a presentation, Journal of Marine Systems, 17(1), 555–569, doi:10.1016/S0924-7963(98)00064-5, 1998.

Kaufman, A., Trier, R. M., Broecker, W. S. and Feely, H. W.: Distribution of 228Ra in the world ocean, Journal of Geophysical Research, 78(36), 8827–8848, doi:10.1029/JC078i036p08827, 1973.

Korb, R. E., Whitehouse, M. J. and Ward, P.: SeaWiFS in the southern ocean: spatial and temporal variability in phytoplankton biomass around South Georgia, Deep Sea Research Part II: Topical Studies in Oceanography, 51(1–3), 99–116, doi:10.1016/j.dsr2.2003.04.002, 2004.

Martin, J. H., Fitzwater, S. E. and Gordon, R. M.: Iron deficiency limits phytoplankton growth in Antarctic waters, Global Biogeochemical Cycles, 4(1), 5–12, doi:10.1029/GB004i001p00005, 1990.

van der Merwe, P., Bowie, A. R., Quéroué, F., Armand, L., Blain, S., Chever, F., Davies, D., Dehairs, F., Planchon, F., Sarthou, G., Townsend, A. T. and Trull, T.: Sourcing the iron in the naturally-fertilised bloom around the Kerguelen Plateau: particulate trace metal dynamics, Biogeosciences Discuss., 11(9), 13389–13432, doi:10.5194/bgd-11-13389-2014, 2014.

Mongin, M. M., Abraham, E. R. and Trull, T. W.: Winter advection of iron can explain the summer phytoplankton bloom that extends 1000 km downstream of the Kerguelen Plateau in the Southern Ocean, Journal of Marine Research, 67(2), 225–237, doi:10.1357/002224009789051218, 2009.

Moore, J. K. and Abbott, M. R.: Surface chlorophyll concentrations in relation to the Antarctic Polar Front: seasonal and spatial patterns from satellite observations, Journal of Marine Systems, 37(1–3), 69–86, doi:10.1016/S0924-7963(02)00196-3, 2002.

Moore, W. S.: Ages of continental shelf waters determined from 223Ra and 224Ra, Journal of Geophysical Research, 105(C9), 22117, doi:10.1029/1999JC000289, 2000.

Moore, W. S.: Fifteen years experience in measuring 224Ra and 223Ra by delayed-coincidence counting, Marine Chemistry, 109(3-4), 188–197, doi:10.1016/j.marchem.2007.06.015, 2008.

Moore, W. S. and Arnold, R.: Measurement of 223Ra and 224Ra in coastal waters using a delayed coincidence counter, Journal of Geophysical Research: Oceans, 101(C1), 1321–1329, doi:10.1029/95JC03139, 1996.

Orsi, A. H., Whitworth III, T. and Nowlin Jr., W. D.: On the meridional extent and fronts of the Antarctic Circumpolar Current, Deep Sea Research Part I: Oceanographic Research Papers, 42(5), 641–673, doi:10.1016/0967-0637(95)00021-W, 1995.

d' Ovidio, F., De Monte, S., Alvain, S., Dandonneau, Y. and Levy, M.: Fluid dynamical niches of phytoplankton types, Proc Natl Acad Sci U S A, 107(43), 18366–18370, doi:10.1073/pnas.1004620107, 2010.

Park, Charriaud E. and Fieux M.: Thermohaline structure of the Antarctic Surface Water/Winter Water in the Indian sector of the Southern Ocean, Journal of Marine Systems, 17(1), 5–23, doi:10.1016/S0924-7963(98)00026-8, 1998a.

Park, Y.-H., Charriaud, E., Pino, D. R. and Jeandel, C.: Seasonal and interannual variability of the mixed layer properties and steric height at station KERFIX, southwest of Kerguelen, Journal of Marine Systems, 17(1-4), 571–586, doi:10.1016/S0924-7963(98)00065-7, 1998b.

Park, Y.-H., Durand, I., Kestenare, E., Rougier, G., Zhou, M., D' Ovidio, F., Cotté, C. and Lee, J.-H.: Polar Front around the Kerguelen Islands: An up-to-date determination and associated circulation of surface/subsurface waters, J. Geophys. Res. Oceans, doi:10.1002/2014JC010061, 2014.

Park, Y.-H., Fuda, J.-L., Durand, I. and Naveira Garabato, A. C.: Internal tides and vertical mixing over the Kerguelen Plateau, Deep Sea Research Part II: Topical Studies in Oceanography, 55(5-7), 582–593, doi:10.1016/j.dsr2.2007.12.027, 2008a.

Park, Y.-H. and Gamberoni, L.: Cross-frontal exchange of Antarctic Intermediate Water and Antarctic Bottom Water in the Crozet Basin, Deep Sea Research Part II: Topical Studies in Oceanography, 44(5), 963–986, doi:10.1016/S0967-0645(97)00004-0, 1997.

Park, Y.-H. and Gambéroni, L.: Large-scale circulation and its variability in the south Indian Ocean from TOPEX/POSEIDON altimetry, Journal of Geophysical Research: Oceans, 100(C12), 24911–24929, doi:10.1029/95JC01962, 1995.

Park, Y.-H., Gamberoni, L. and Charriaud, E.: Frontal structure, water masses, and circulation in the Crozet Basin, Journal of Geophysical Research, 98(C7), 12361, doi:10.1029/93JC00938, 1993.

Park, Y.-H., Roquet, F., Durand, I. and Fuda, J.-L.: Large-scale circulation over and around the Northern Kerguelen Plateau, Deep Sea Research Part II: Topical Studies in Oceanography, 55(5-7), 566–581, doi:10.1016/j.dsr2.2007.12.030, 2008b.

Park, Y.-H., Vivier, F., Roquet, F. and Kestenare, E.: Direct observations of the ACC transport across the Kerguelen Plateau, Geophysical Research Letters, 36(18), doi:10.1029/2009GL039617, 2009.

Pollard, R. ., Lucas, M. . and Read, J. .: Physical controls on biogeochemical zonation in the Southern Ocean, Deep Sea Research Part II: Topical Studies in Oceanography, 49(16), 3289–3305, doi:10.1016/S0967-0645(02)00084-X, 2002.

Pollard, R., Sanders, R., Lucas, M. and Statham, P.: The Crozet Natural Iron Bloom and Export Experiment (CROZEX), Deep Sea Research Part II: Topical Studies in Oceanography, 54(18–20), 1905–1914, doi:10.1016/j.dsr2.2007.07.023, 2007.

Quéroué, F., Sarthou, G., Planquette, H.F., Bucciarelli, F., Chever, F., van der Merwe, P., Lannuzel, D., Townsend, A.T., Cheize, M., Blain, S., d'Ovidio, F. and Bowie, A.: High variability of dissolved iron concentrations in the vicinity of Kerguelen Island (Southern Ocean) submitted to Biogeosciences.

Sanial, V., Van Beek, P., Lansard, B., D' Ovidio, F., Kestenare, E., Souhaut, M., Zhou, M. and Blain, S.: Study of the phytoplankton plume dynamics off the Crozet Islands (Southern Ocean): A geochemical-physical coupled approach, J. Geophys. Res. Oceans, 119, 2227–2237, doi:10.1002/2013JC009305, 2014.

Tagliabue, A., Sallée, J.-B., Bowie, A. R., Lévy, M., Swart, S. and Boyd, P. W.: Surface-water iron supplies in the Southern Ocean sustained by deep winter mixing, Nature Geosci, 7(4), 314–320, doi:10.1038/ngeo2101, 2014.

van Beek, P., Bourquin, M., Reyss, J.-L., Souhaut, M., Charette, M. A. and Jeandel, C.: Radium isotopes to investigate the water mass pathways on the Kerguelen Plateau (Southern Ocean), Deep Sea Research Part II: Topical Studies in Oceanography, 55(5-7), 622–637, doi:10.1016/j.dsr2.2007.12.025, 2008.

van Beek, P., Souhaut, M., Lansard, B., Bourquin, M., Reyss, J.-L., Von Ballmoos, P. and Jean, P.: LAFARA: a new underground laboratory in the French Pyrenees for ultra low-level gamma-ray spectrometry, J. Environ. Radioact., 116, 152–158, doi:10.1016/j.jenvrad.2012.10.002, 2013.

van Beek, P., Souhaut, M. and Reyss, J.-L.: Measuring the radium quartet (228Ra, 226Ra, 224Ra, 223Ra) in seawater samples using gamma spectrometry, Journal of Environmental Radioactivity, 101(7), 521–529, doi:10.1016/j.jenvrad.2009.12.002, 2010.

Weis, D. and Frey, F. A.: Submarine Basalts of the Northern Kerguelen Plateau: Interaction Between the Kerguelen Plume and the Southeast Indian Ridge Revealed at ODP Site 1140, J. Petrology, 43(7), 1287–1309, doi:10.1093/petrology/43.7.1287, 2002.

Zhang, Y., Lacan, F. and Jeandel, C.: Dissolved rare earth elements tracing lithogenic inputs over the Kerguelen Plateau (Southern Ocean), Deep Sea Research Part II: Topical Studies in Oceanography, 55(5–7), 638–652, doi:10.1016/j.dsr2.2007.12.029, 2008.

Zhou, M., Zhu, Y., D' Ovidio, F., Park, Y.-H., Durand, I., Kestenare, E., Sanial, V., Van-Beek, P., Queguiner, B., Carlotti, F. and Blain, S.: Surface currents and upwelling in Kerguelen Plateau regions, Biogeosciences Discuss., 11(5), 6845–6876, doi:10.5194/bgd-11-6845-2014, 2014.

Table 1: Dissolved ^{223}Ra, ^{224}Ra and ^{228}Ra activities determined in surface samples collected off the Kerguelen Islands. The ^{223}Ra and ^{224}Ra activities are excess radium activities (see Methods for details). Activities are expressed in disintegration per minute per 100 L (dpm/ 100 L). <DL = Below the Detection Limit.

Table 2: Dissolved ^{223}Ra, ^{224}Ra and ^{228}Ra activities determined in seawater samples collected in the water column using Niskin bottles. The ^{223}Ra and ^{224}Ra activities are excess radium activities (See Methods for details). Activities are expressed in disintegration per minute per 100 L (dpm/ 100 L). The number of counts detected using the RaDeCC is also reported in the Table (cnts). <DL = Below the Detection Limit.

Station	Sampling	Volume	Depth	Bottom Depth	^{223}Ra	^{224}Ra	^{228}Ra	$^{223}Ra/^{228}Ra$	$^{224}Ra/^{228}Ra$	$^{224}Ra/^{223}Ra$
	Date	(L)	(m)	(m)	(dpm/ 100 L)	(dpm/ 100 L)	(dpm/ 100 L)			
UW-14	17/10/2011 12:10	900	7	342	< LD	< LD	0.06 ± 0.019			
UW-15	18/10/2011 05:43	900	7	712	0.008 ± 0.006	< LD	0.03 ± 0.010	0.24 ± 0.19		
UW-16	18/10/2011 09:50	900	7	560	0.007 ± 0.007	< LD	0.05 ± 0.013	0.13 ± 0.13		
UW-17	19/10/2011 22:03	500	7	676	< LD	< LD	0.17 ± 0.035			
UW-18	19/10/2011 01:30	250	7	104	0.062 ± 0.018	0.213 ± 0.062	0.49 ± 0.079	0.13 ± 0.04	0.44 ± 0.15	3.45 ± 1.41
UW-19	19/10/2011 01:30	250	7	160	0.047 ± 0.016	0.143 ± 0.052	0.47 ± 0.139	0.10 ± 0.05	0.31 ± 0.14	3.03 ± 1.51
UW-20	19/10/2011 04:15	250	7		0.090 ± 0.020	0.808 ± 0.079	1.21 ± 0.082	0.07 ± 0.02	0.67 ± 0.08	8.98 ± 2.15
UW-21	24/10/2011 10:46	700	7	597	0.011 ± 0.005	0.036 ± 0.024	0.11 ± 0.026	0.10 ± 0.05	0.33 ± 0.24	3.38 ± 2.69
UW-22	24/10/2011 12:10	450	7	253	0.023 ± 0.007	< LD	0.20 ± 0.039	0.11 ± 0.04		
UW-23	24/10/2011 14:05	450	7	233	0.008 ± 0.006	0.116 ± 0.025	0.04 ± 0.013	0.19 ± 0.16	2.92 ± 1.16	15.17 ± 11.93
UW-24	24/10/2011 23:37	450	7	171	< LD	< LD	0.11 ± 0.020			
UW-25	28/10/2011 03:40	700	7	116	0.060 ± 0.011	0.218 ± 0.055	0.08 ± 0.017	0.72 ± 0.19	2.62 ± 0.84	3.64 ± 1.11
UW-26	28/10/2011 04:35	700	7	130	0.043 ± 0.010	0.065 ± 0.033	0.19 ± 0.023	0.23 ± 0.06	0.34 ± 0.18	1.50 ± 0.84
UW-27	28/10/2011 06:00	500	7	393	0.019 ± 0.007	< LD	0.06 ± 0.016	0.31 ± 0.14		
UW-28	28/10/2011 06:55	700	7	650	0.020 ± 0.008	< LD	0.07 ± 0.015	0.29 ± 0.13		
UW-29	31/10/2011 07:44	450	7	100	0.031 ± 0.011	0.118 ± 0.045	0.53 ± 0.038	0.06 ± 0.02	0.22 ± 0.09	3.81 ± 2.02
UW-30	31/10/2011 08:17	450	7	100	0.083 ± 0.014	0.201 ± 0.039	0.58 ± 0.039	0.14 ± 0.03	0.35 ± 0.07	2.44 ± 0.62
UW-31	05/11/2011 12:20	700	7		< LD	< LD	0.17 ± 0.027			
UW-32	08/11/2011 08:50	700	7	4561	0.013 ± 0.008	0.035 ± 0.046	0.24 ± 0.040	0.05 ± 0.04	0.15 ± 0.19	2.82 ± 4.10
UW-33	08/11/2011 13:17	450	7	1664	< LD	< LD	0.09 ± 0.030			
UW-34	09/11/2011 01:50	500	7	1118	0.017 ± 0.011	0.124 ± 0.078	0.10 ± 0.020	0.16 ± 0.12	1.23 ± 0.80	7.45 ± 6.84
UW-35	17/11/2011 16:41	700	7	554	< LD	< LD	0.16 ± 0.026			
UW-36	21/11/2011 05:25	500	7	21	0.098 ± 0.016	0.411 ± 0.098	1.07 ± 0.054	0.09 ± 0.02	0.38 ± 0.09	4.18 ± 1.22
UW-37	22/11/2011 08:35	900	7	3720	< LD	< LD	0.13 ± 0.016			
TNS-1	23/10/2011 11:55	500	7	2280	0.015 ± 0.005	0.046 ± 0.033	0.07 ± 0.022	0.21 ± 0.10	0.65 ± 0.50	3.11 ± 2.46
TNS-2	23/10/2011 07:00	700	7	520	0.023 ± 0.006	< LD	0.31 ± 0.064	0.07 ± 0.02		
TNS-3	23/10/2011 03:23	700	7	540	0.006 ± 0.004	< LD	0.15 ± 0.050	0.04 ± 0.03		
TNS-4	22/10/2011 19:30	700	7	1800	0.015 ± 0.005	< LD	0.08 ± 0.017	0.20 ± 0.08		
TNS-5	22/10/2011 11:55	700	7	2060	0.021 ± 0.005	0.070 ± 0.030	0.17 ± 0.050	0.13 ± 0.05	0.42 ± 0.22	3.26 ± 1.62
TNS-7	21/10/2011 20:25	700	7	1864	< LD	< LD	0.03 ± 0.012			
TEW-1	31/10/2011 05:56	700	7	92	0.014 ± 0.011	0.131 ± 0.045	0.84 ± 0.051	0.02 ± 0.01	0.16 ± 0.05	9.31 ± 7.86
TEW-2	31/10/2011 10:40	450	7	85	0.039 ± 0.011	0.153 ± 0.045	0.28 ± 0.027	0.14 ± 0.04	0.55 ± 0.17	3.89 ± 1.56
TEW-3	31/10/2011 17:35	500	7	557	0.008 ± 0.007	< LD	0.10 ± 0.018	0.08 ± 0.07		
TEW-4	01/11/2011 03:45	500	7	1596	< LD	< LD	0.08 ± 0.025			
TEW-5	01/11/2011 16:05	450	7	2290	< LD	0.128 ± 0.044	0.18 ± 0.033		0.71 ± 0.28	
TEW-6	02/11/2011 00:05	450	7	2400	0.011 ± 0.006	< LD	0.08 ± 0.019	0.13 ± 0.08		
TEW-7	02/11/2011 05:15	700	7	2510	0.020 ± 0.009	0.147 ± 0.062	0.16 ± 0.019	0.13 ± 0.06	0.93 ± 0.40	7.37 ± 4.51
TEW-8	02/11/2011 17:40	900	7	2800	< LD	< LD	0.17 ± 0.024			
E-1	29/10/2011 10:55	900	7	2065	0.021 ± 0.005	0.070 ± 0.022	0.10 ± 0.022	0.23 ± 0.08	0.73 ± 0.28	3.26 ± 1.29
E-3	03/11/2011 16:15	900	7	1915	0.009 ± 0.005	< LD	0.03 ± 0.016	0.33 ± 0.25		
E-4W	12/11/2011 06:15	900	7	1385	0.010 ± 0.007	< LD	0.14 ± 0.034			
E-4E	12/11/2011 08:37	500	7	2210	< LD	< LD	0.12 ± 0.021			
E-5	18/11/2011 00:25	900	7	1920	< LD	< LD	0.11 ± 0.008			
A3-1	19/10/2011 19:15	900	7	528	0.015 ± 0.003	0.034 ± 0.024	0.12 ± 0.041	0.12 ± 0.05	0.28 ± 0.21	2.26 ± 1.62
A3-2	19/10/2011 19:15	900	7	531	< LD	< LD	0.12 ± 0.024			
G-1	09/11/2011 05:20	900	7	592	0.023 ± 0.007	< LD	0.05 ± 0.020	0.46 ± 0.23		
G-2	09/11/2011 14:10	500	7	67	0.089 ± 0.015	0.412 ± 0.052	0.36 ± 0.046	0.25 ± 0.05	1.15 ± 0.21	4.64 ± 0.98
G-2b	21/11/2011 11:00	500	7	67	0.130 ± 0.017	0.568 ± 0.067	0.75 ± 0.066	0.17 ± 0.03	0.75 ± 0.11	4.36 ± 0.77
F-L	06/11/2011 13:33	900	7	2670	< LD	< LD	0.17 ± 0.021			
R-2	26/10/2011 02:40	900	7	2531	0.016 ± 0.009	0.057 ± 0.028	0.11 ± 0.016	0.15 ± 0.09	0.53 ± 0.27	3.49 ± 2.51
KER-1	19/10/2011 04:45	87.8	1	3	0.302 ± 0.048	2.053 ± 0.125	1.62 ± 0.160	0.19 ± 0.03	1.27 ± 0.15	6.80 ± 1.16
BaieB-1	31/10/2011 05:00	99.3	1	3	0.219 ± 0.032	2.332 ± 0.118	0.88 ± 0.089	0.25 ± 0.04	2.65 ± 0.30	10.67 ± 1.67
BaieB-2	40847.20833	65.2	1	3	0.012 ± 0.008	0.256 ± 0.024	2.57 ± 0.183	0.005 ± 0.003	0.10 ± 0.01	20.64 ± 13.83

Station and Depth (m)	Volume (L)	Bottom Depth (m)	^{223}Ra (dpm/ 100 L)	^{223}Ra cnts	^{224}Ra (dpm/ 100 L)	^{224}Ra cnts	^{228}Ra (dpm/ 100 L)	^{228}Ra cnts
E-1								
182	256	2065	< LD		0.041 ± 0.031	134	0.03 ± 0.01	44
508	263	2065	0.019 ± 0.012	38	< LD		< LD	
1013	262	2065	0.010 ± 0.009	24	< LD		0.07 ± 0.015	78
1623	256	2065	0.058 ± 0.013	74	< LD		0.22 ± 0.034	134
2069	274	2065	0.170 ± 0.024	180	0.045 ± 0.037	344	0.23 ± 0.033	141
TEW-3								
101	259	557	< LD		< LD		0.29 ± 0.068	125
303	257	557	0.039 ± 0.013	37	0.065 ± 0.052	129	0.28 ± 0.037	154
557	252	557	0.014 ± 0.015	33	0.077 ± 0.056	213	0.37 ± 0.098	68
F-L								
101	257	2670	0.008 ± 0.007	17	< LD		0.20 ± 0.130	49
183	260	2670	< LD		0.086 ± 0.022	246	0.19 ± 0.054	35
405	258	2670	0.016 ± 0.009	24	< LD		0.06 ± 0.030	22
907	258	2670	0.039 ± 0.012	46	0.103 ± 0.060	107	0.12 ± 0.044	28
1825	122	2670	0.064 ± 0.017	32	0.128 ± 0.077	239	0.54 ± 0.130	49
2723	124	2670	0.142 ± 0.049	123	0.265 ± 0.154	346	0.93 ± 0.097	290
G-1								
10	269	592	< LD		< LD		0.38 ± 0.042	187
53	251	592	0.020 ± 0.009	30	0.051 ± 0.049	107	0.31 ± 0.039	157
130	255	592	< LD		< LD		0.26 ± 0.066	43
303	260	592	< LD		< LD		0.38 ± 0.081	56
455	234	592	< LD		< LD		0.29 ± 0.074	44
576	223	592	0.088 ± 0.021	84	0.075 ± 0.058	75	0.36 ± 0.077	48
E-4W								
94	261	1385	0.020 ± 0.014	31	< LD		0.34 ± 0.079	50
192	260	1385	< LD		< LD		0.30 ± 0.041	135
608	253	1385	< LD		< LD		0.29 ± 0.043	151
1013	123	1385	< LD		0.133 ± 0.046	93	0.43 ± 0.116	36
1383	123	1385	0.057 ± 0.021	25	0.071 ± 0.046	145	0.90 ± 0.164	59
A3-2								
101	258	531	< LD		< LD		0.10 ± 0.042	25
152	246	531	< LD		< LD		0.16 ± 0.029	115
233	258	531	< LD		< LD		0.18 ± 0.060	33
303	124	531	< LD		< LD		0.49 ± 0.125	39
404	110	531	< LD		< LD		0.68 ± 0.156	44
518	246	531	0.081 ± 0.019	58	< LD		0.70 ± 0.102	82
TEW-1								
82	258.5	92	0.053 ± 0.015	49	0.125 ± 0.059	334	0.88 ± 0.083	197
TEW-8								
20	269	2800	0.011 ± 0.009	22	< LD	335	0.14 ± 0.032	69
G-2								
50	229.6	67	0.094 ± 0.022	65	0.737 ± 0.097	389	0.79 ± 0.083	167

Fig. 1.

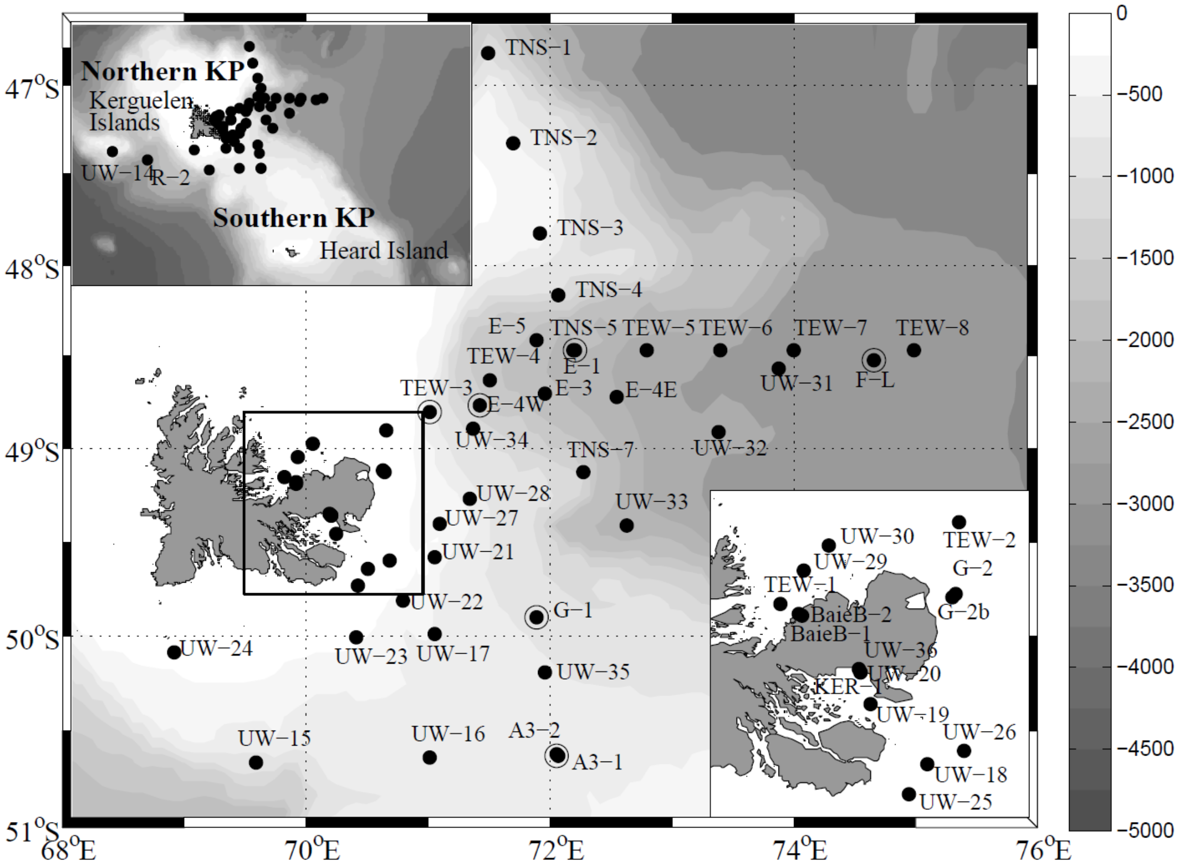

Northern KP
Kerguelen Islands
UW−14
R−2
Southern KP
Heard Island
TNS−1
TNS−2
TNS−3
TNS−4
E−5
TNS−5
TEW−5
TEW−6
TEW−7
TEW−8
TEW−4
E−1
UW−31
F−L
TEW−3
E−3
E−4E
E−4W
UW−34
TNS−7
UW−32
UW−28
UW−27
UW−33
UW−21
UW−22
G−1
UW−24
UW−23
UW−17
UW−35
UW−15
UW−16
A3−2
A3−1
UW−30
TEW−2
UW−29
G−2
TEW−1
BaieB−2
G−2b
BaieB−1
UW−36
UW−20
KER−1
UW−19
UW−26
UW−18
UW−25
47°S
48°S
49°S
50°S
51°S
68°E
70°E
72°E
74°E
76°E
0
−500
−1000
−1500
−2000
−2500
−3000
−3500
−4000
−4500
−5000

Fig. 2.

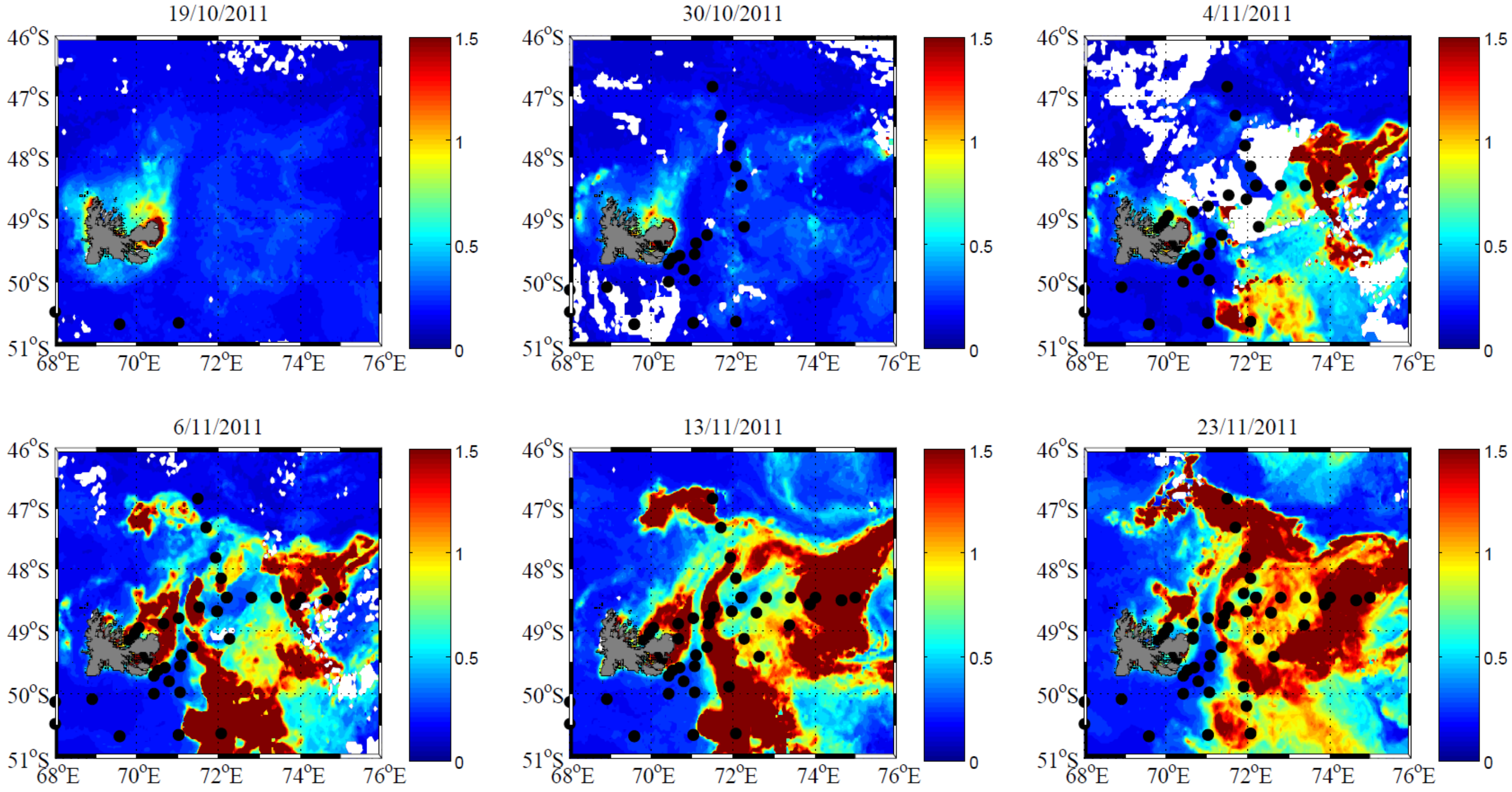
19/10/2011
30/10/2011
4/11/2011
6/11/2011
13/11/2011
23/11/2011
46°S
47°S
48°S
49°S
50°S
51°S
68°E
70°E
72°E
74°E
76°E
0
0.5
1
1.5

Fig. 3.

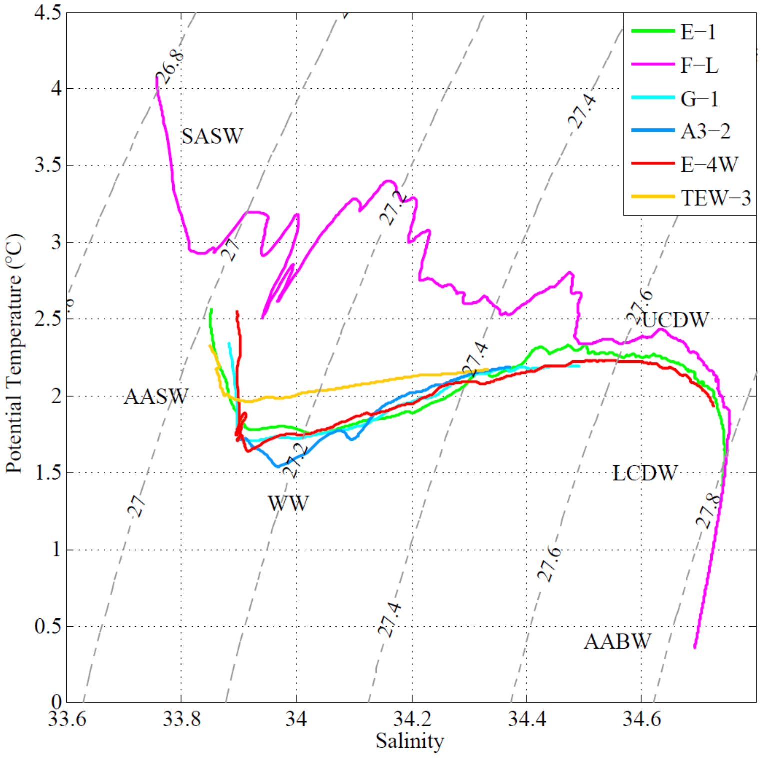
E−1
F−L
G−1
A3−2
E−4W
TEW−3
SASW
AASW
WW
UCDW
LCDW
AABW
Potential Temperature (°C)
Salinity
26.8
27
27.2
27.4
27.6
27.8
4.5
4
3.5
3
2.5
2
1.5
1
0.5
0
33.6
33.8
34
34.2
34.4
34.6

Fig. 4.

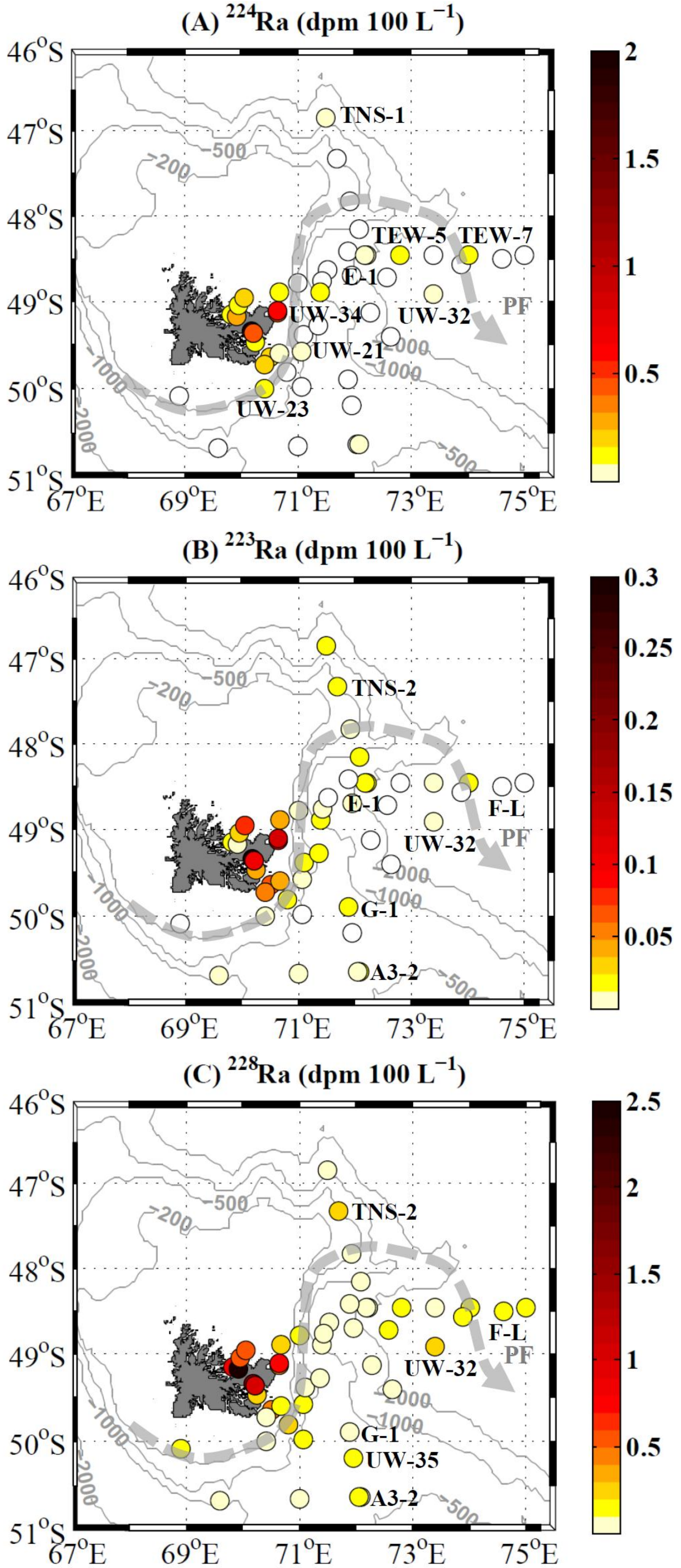
(A) ²²⁴Ra (dpm 100 L⁻¹)
TNS-1
TEW-5
TEW-7
E-1
UW-34
UW-32
UW-21
UW-23
PF
-500
-200
-1000
-2000
2
1.5
1
0.5
(B) ²²³Ra (dpm 100 L⁻¹)
TNS-2
E-1
F-L
UW-32
G-1
A3-2
PF
0.3
0.25
0.2
0.15
0.1
0.05
(C) ²²⁸Ra (dpm 100 L⁻¹)
TNS-2
F-L
UW-32
G-1
UW-35
A3-2
PF
2.5
2
1.5
1
0.5
46°S
47°S
48°S
49°S
50°S
51°S
67°E
69°E
71°E
73°E
75°E

Fig. 5.

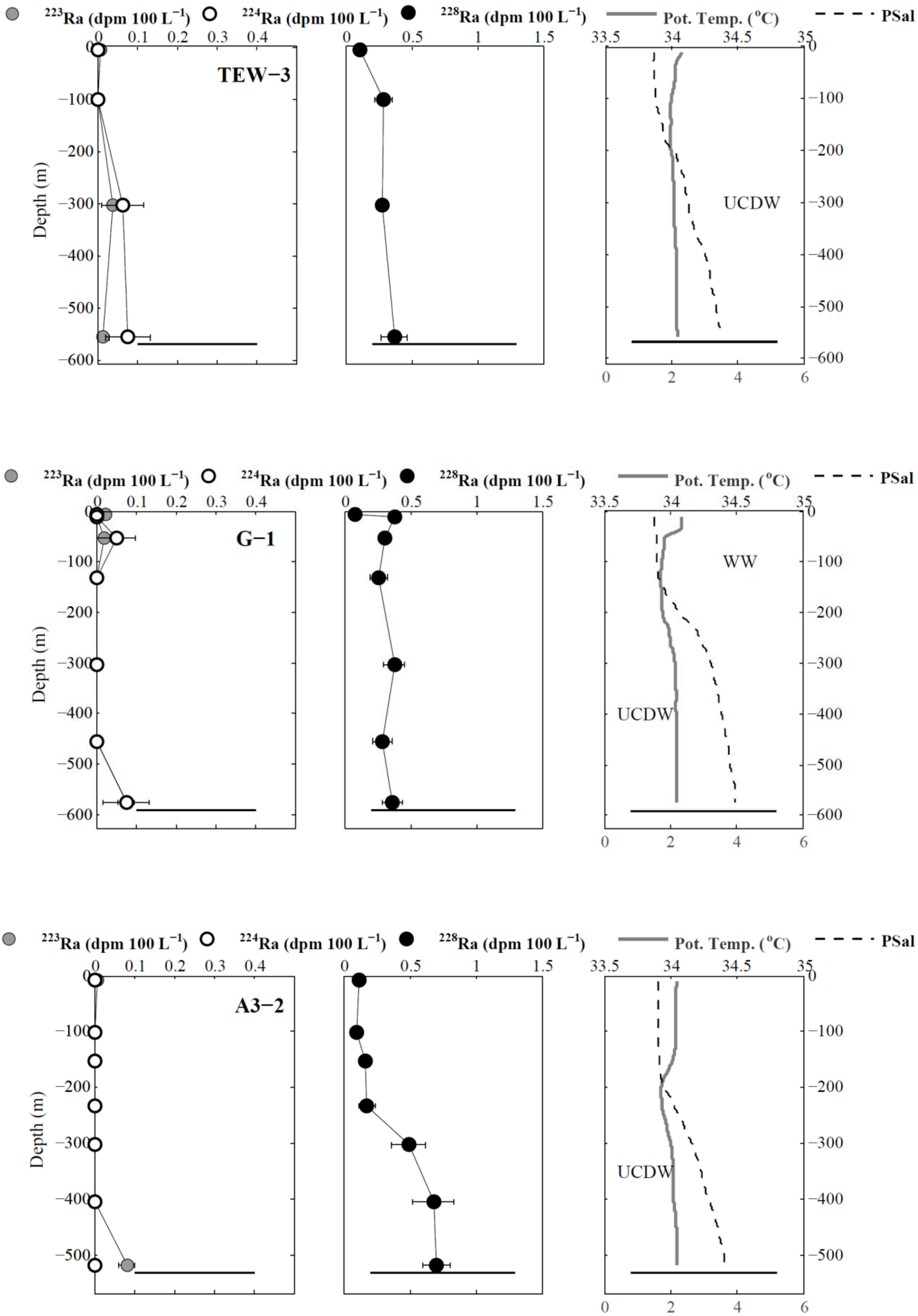

223Ra (dpm 100 L−1)
224Ra (dpm 100 L−1)
228Ra (dpm 100 L−1)
Pot. Temp. (°C)
PSal
0 0.1 0.2 0.3 0.4
0 0.5 1 1.5
33.5 34 34.5 35
0 2 4 6
Depth (m)
0 −100 −200 −300 −400 −500 −600
TEW−3
UCDW
G−1
WW
UCDW
A3−2
UCDW

Fig. 6.

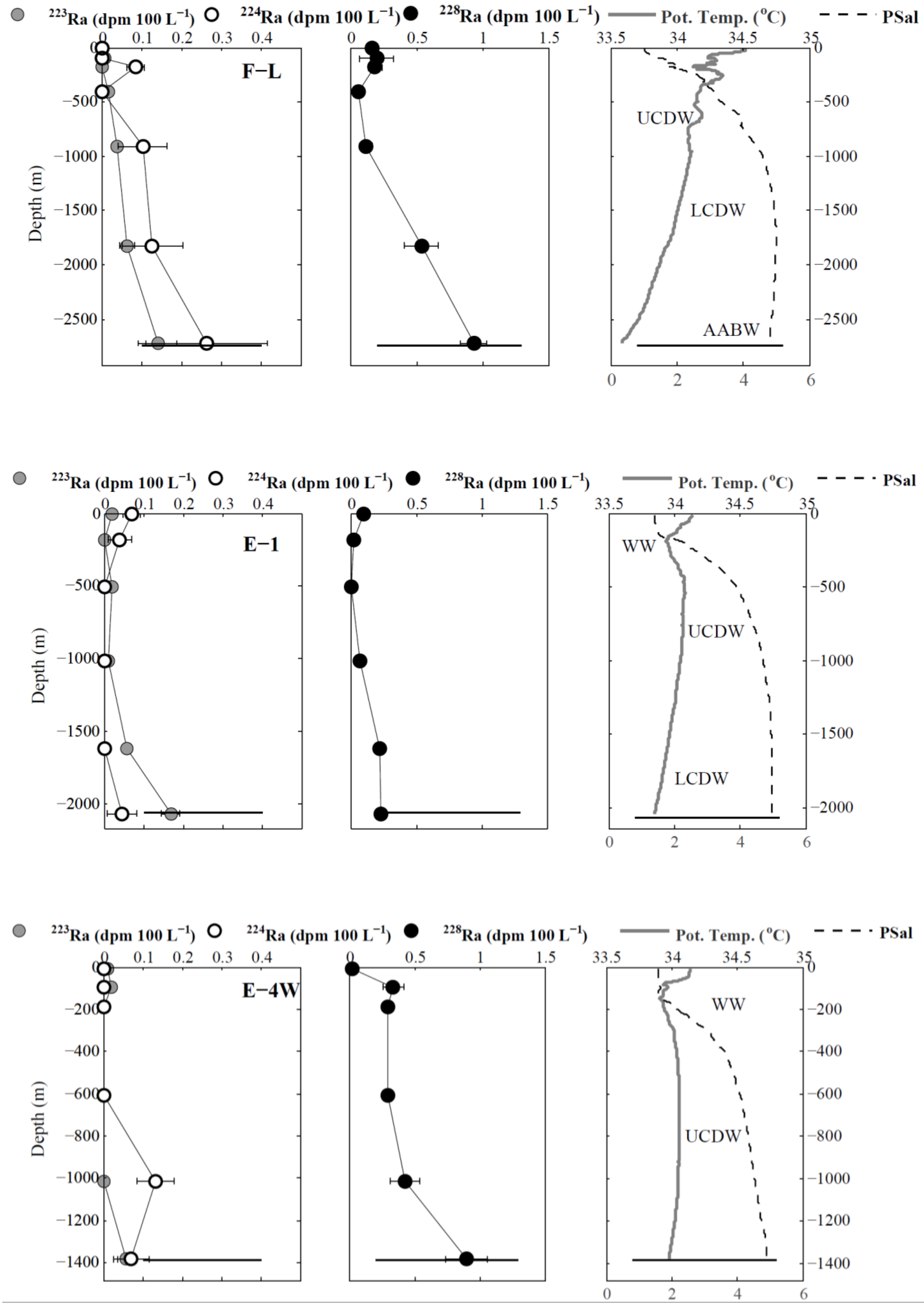
^{223}Ra (dpm 100 L^{-1})
^{224}Ra (dpm 100 L^{-1})
^{228}Ra (dpm 100 L^{-1})
Pot. Temp. (°C)
PSal
F−L
UCDW
LCDW
AABW
Depth (m)
E−1
WW
UCDW
LCDW
Depth (m)
E−4W
WW
UCDW
Depth (m)

Fig. 7.

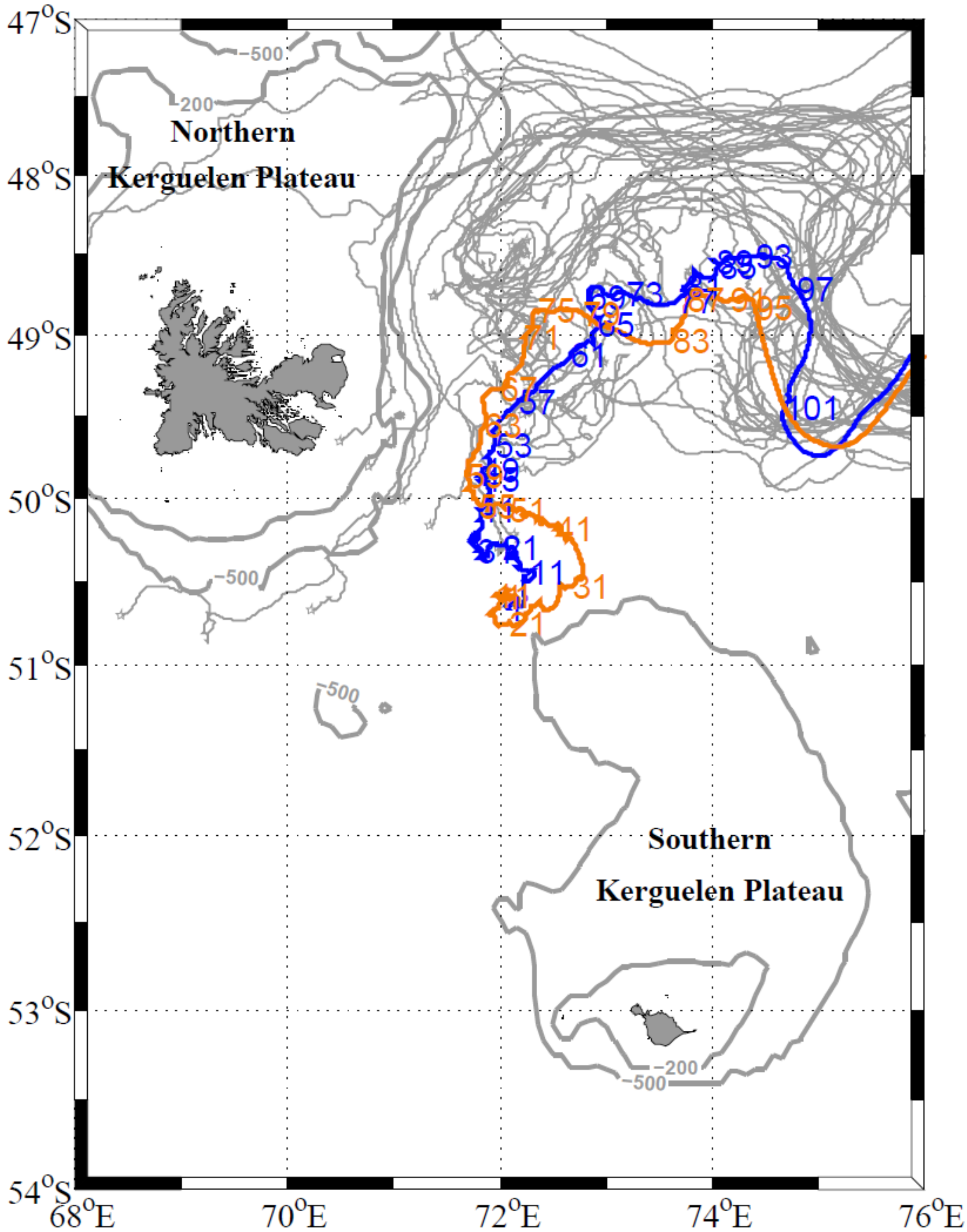
Northern
Kerguelen Plateau
Southern
Kerguelen Plateau
−500
−200
47°S
48°S
49°S
50°S
51°S
52°S
53°S
54°S
68°E
70°E
72°E
74°E
76°E

Fig. 8.

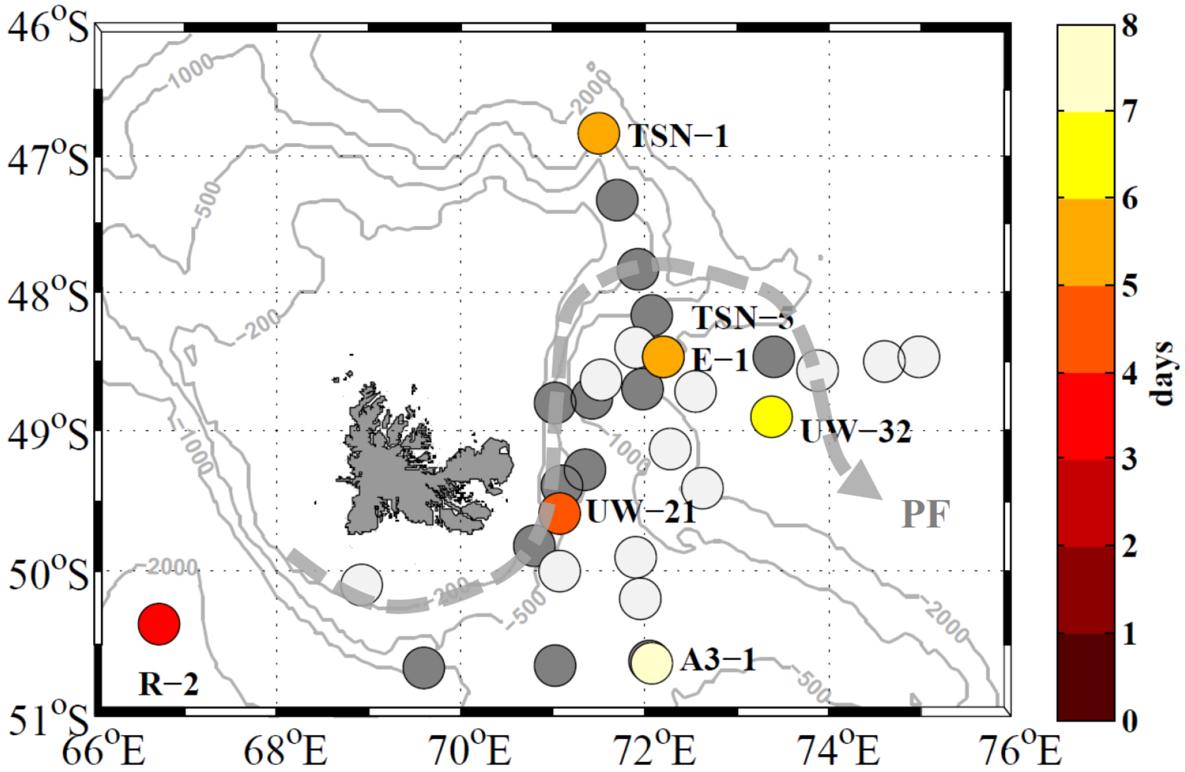
46°S
47°S
48°S
49°S
50°S
51°S
66°E
68°E
70°E
72°E
74°E
76°E
TSN−1
TSN−5
E−1
UW−32
UW−21
A3−1
R−2
PF
1000
500
200
2000
days
0
1
2
3
4
5
6
7
8

Fig. 9.

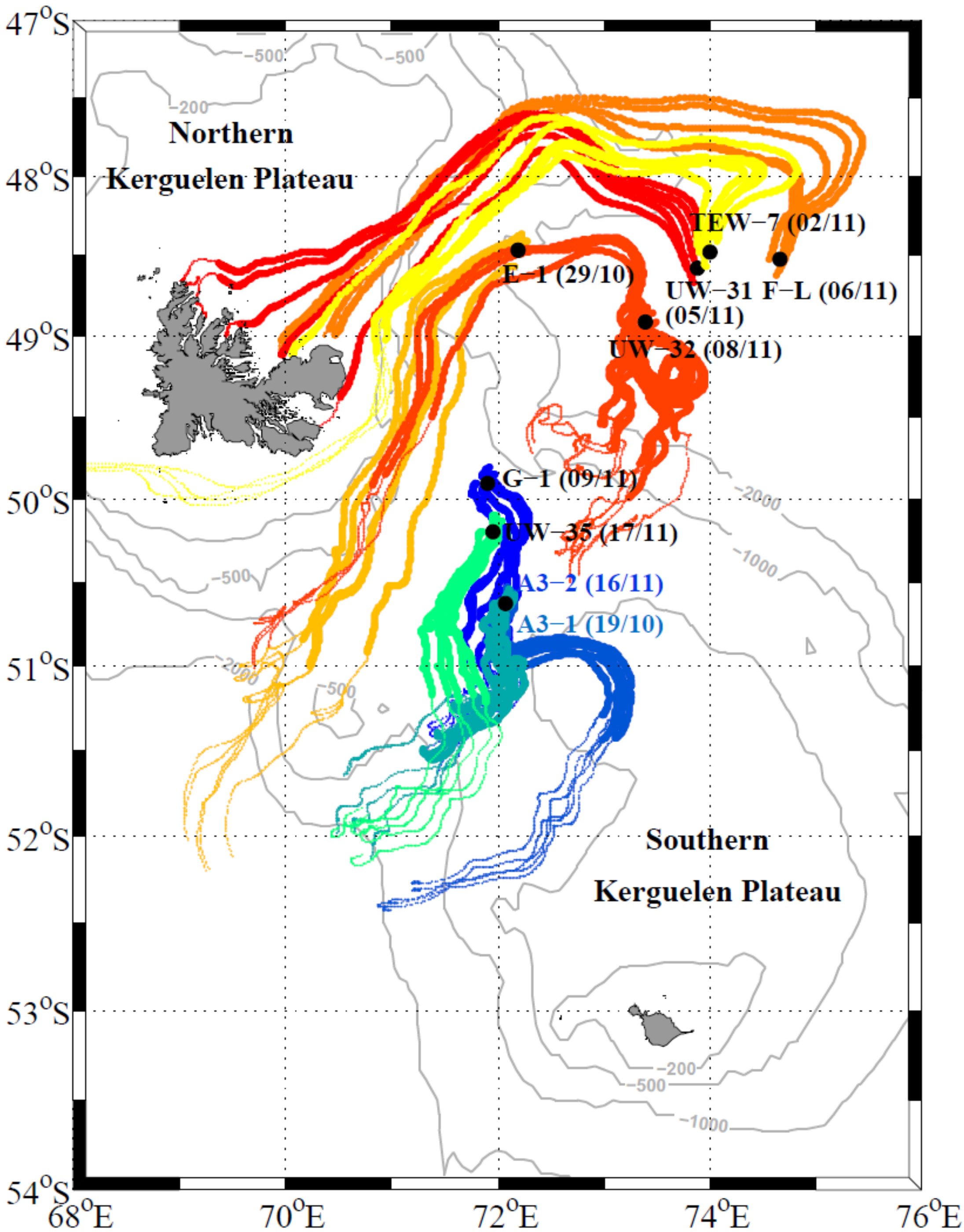

47°S
48°S
49°S
50°S
51°S
52°S
53°S
54°S
68°E
70°E
72°E
74°E
76°E
Northern
Kerguelen Plateau
Southern
Kerguelen Plateau
TEW−7 (02/11)
E−1 (29/10)
UW−31 F−L (06/11)
(05/11)
UW−32 (08/11)
G−1 (09/11)
UW−35 (17/11)
A3−2 (16/11)
A3−1 (19/10)
−200
−500
−1000
−2000

Fig. 10